Supplementary Material

Degeneracy explains diversity in interneuronal regulation of pattern separation in heterogeneous dentate gyrus networks

Sarang Saini and Rishikesh Narayanan*

Cellular Neurophysiology Laboratory, Molecular Biophysics Unit, Indian Institute of Science, Bangalore, India

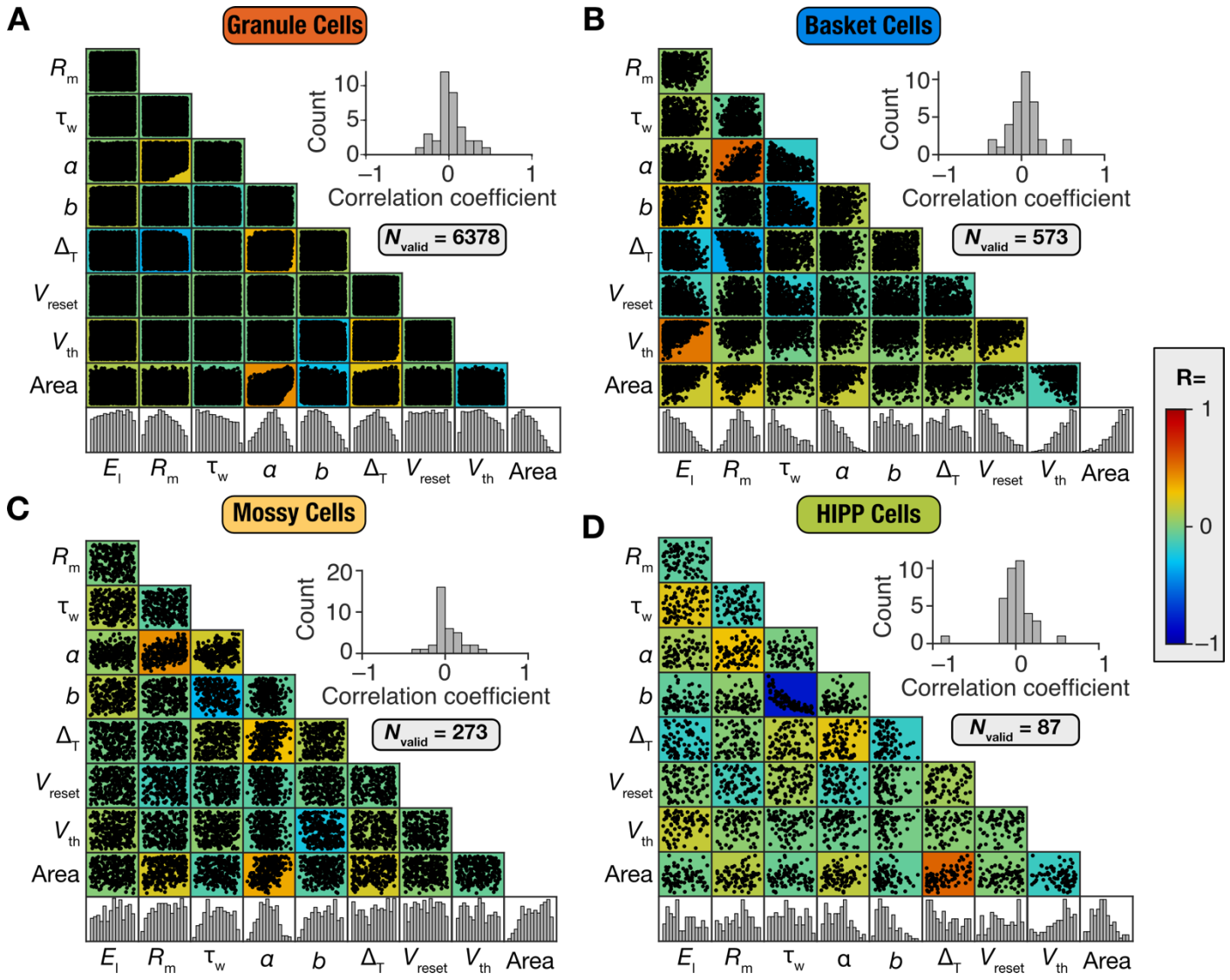

Supplementary Figure S1: Weak pairwise correlations among heterogeneously distributed parameters of model populations of four neuronal subtypes. (A–D) Scatter plot matrix of all parameters from valid populations of granule (A), basket (B), mossy (C), and HIPP (D) cells obtained using MPMOSS. The bottom most rows in each panel indicates the histogram of the specific parameter, showing widespread heterogeneity across models. The insets within each panel depict the histogram of the Pearson's correlation coefficient values, which are overlaid on the respective scatter plot matrices, for the unique correlation coefficient values from the pairwise comparisons shown in the scatter plot matrix. The capacitance value was uniformly set at $1\ \mu\mathrm{F/cm^2}$ across all models and therefore is not included in these plots.

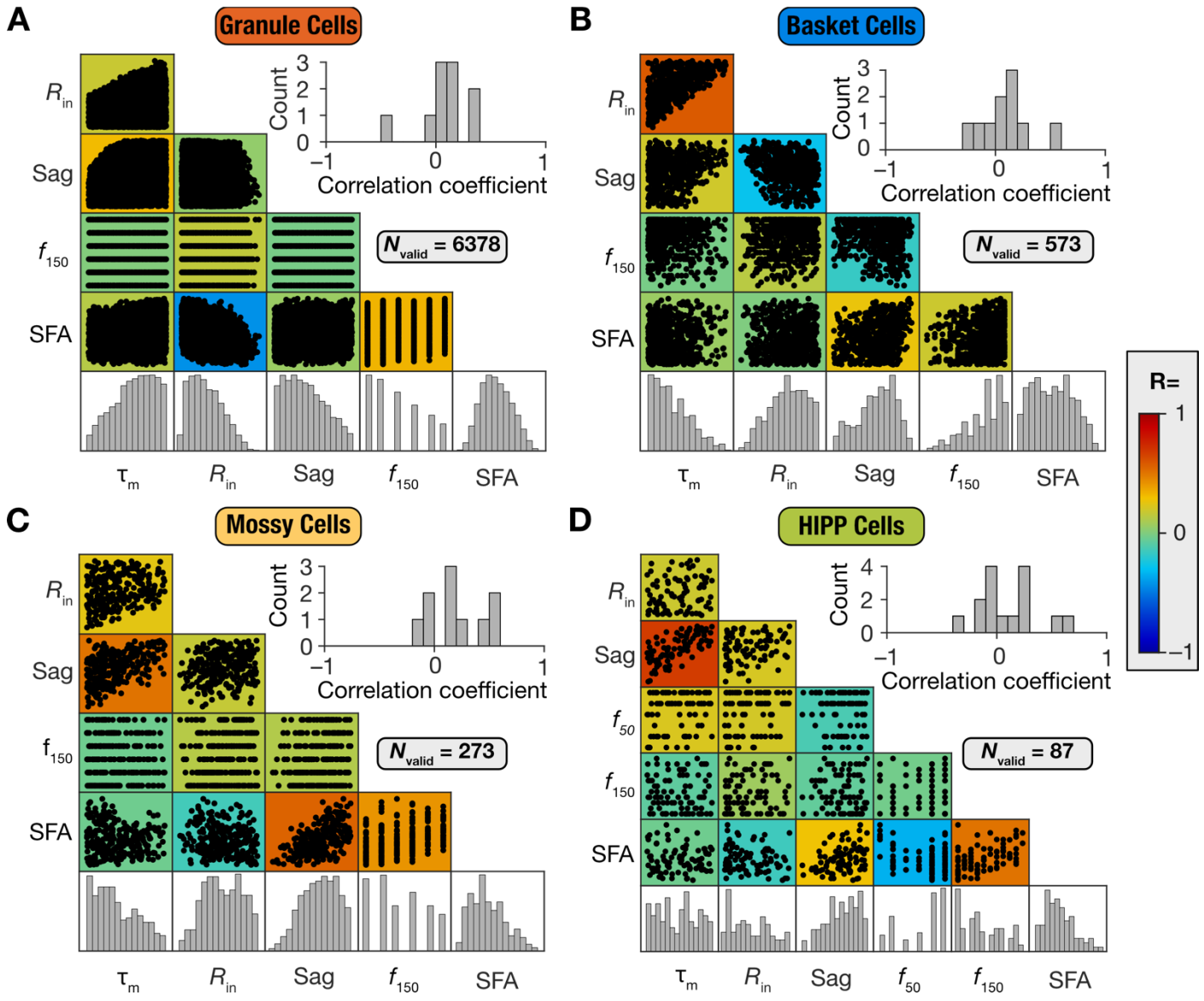

Supplementary Figure S2: Weak pairwise correlations among heterogeneously distributed measurements of model populations of four neuronal subtypes. (A–D) Scatter plot matrix of measurements from valid populations of granule (A), basket (B), mossy (C), and HIPP (D) cells obtained using MPMOSS. The bottom most rows in each panel indicates the histogram of the specific measurement, showing widespread heterogeneity across models. The insets within each panel depict the histogram of the Pearson's correlation coefficient values, which are overlaid on the respective scatter plot matrices, for the unique correlation coefficient values from the pairwise comparisons shown in the scatter plot matrix. The firing rate for 50 pA current injection, f_{50}, was required to be identically zero across all valid GC, BC, and MC models and therefore are not part of these scatter plots.

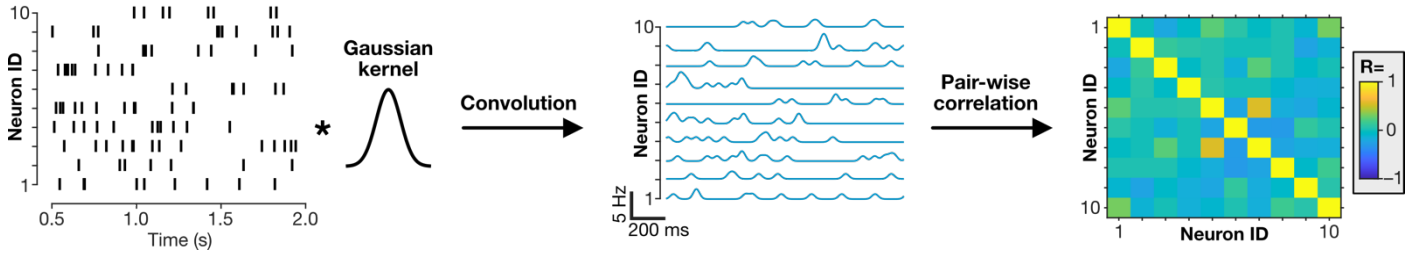

Supplementary Figure S3: Quantification of pattern separation using correlation in instantaneous firing rates (R_β). For calculation of R_β between two patterns, spike times of both the patterns were first convolved with a Gaussian kernel of $\sigma = \frac{1}{10f}$, where f represented the mean firing rate of the population. Then pairwise correlations were computed between each neuron pair, which gave us an $N \times N$ matrix for each pattern. R_β between any two patterns was computed as the correlation coefficient between the matrices associated with the two patterns.

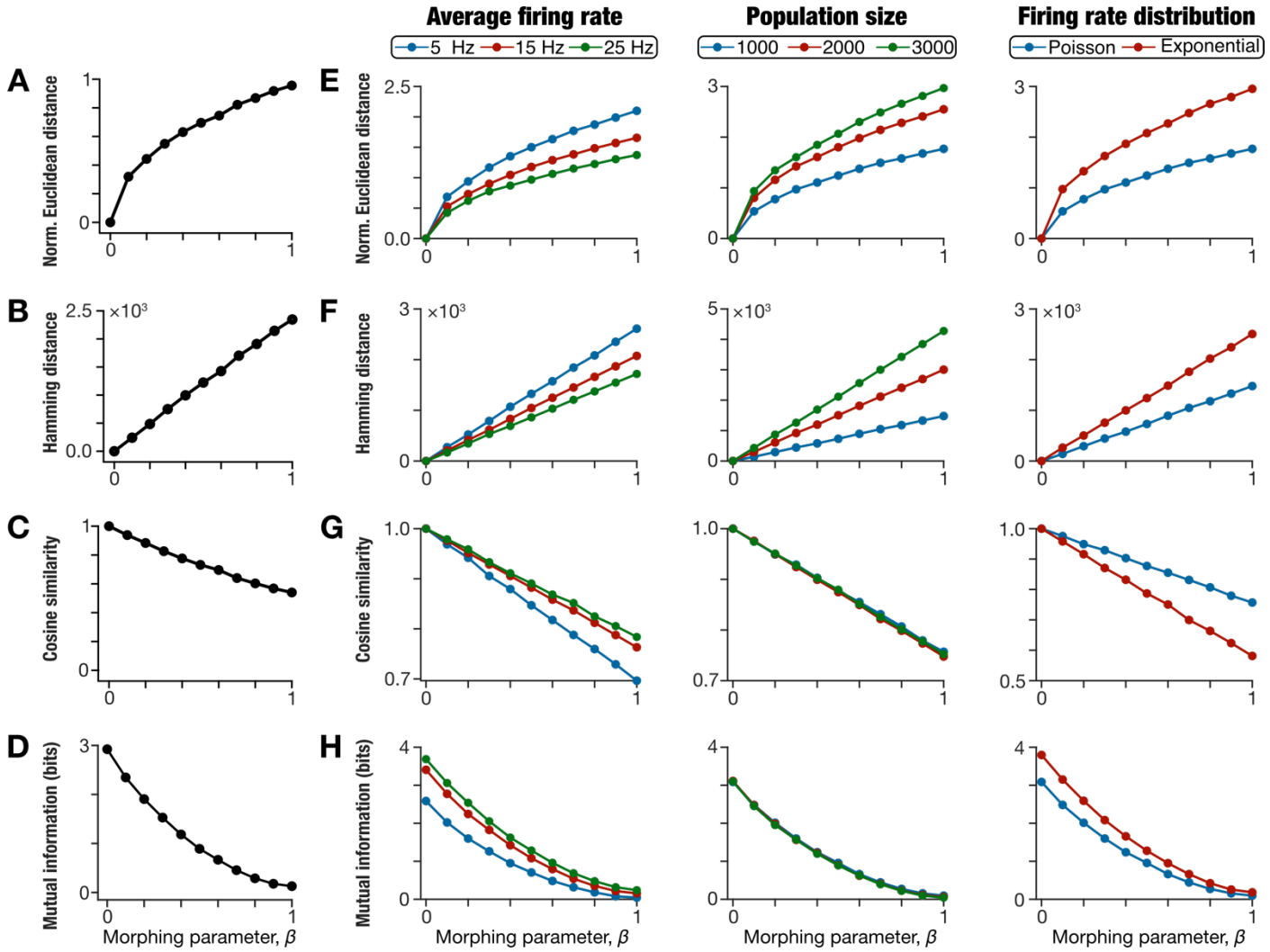

Supplementary Figure S4. Performance of different metrics used to measure similarity of morphed sets of spike trains. (A–D) Assessment of the different distance metrics for comparing the 11 different input patterns, with reference to the P_0 pattern. Shown are the computed distances between P_β (with $0 \leq \beta \leq 1$) and P_0 for normalized Euclidean distance (A), Hamming distance (B), cosine similarity (C), and mutual information (D). (E–H) Performance of 6 different metrics that quantified similarity/dissimilarity of spike raster patterns generated for different average firing rate (*first column*), different population sizes (*second column*), and different firing rate distributions (*third column*). In each scenario, ten sets of two distinct patterns (P_0 and P_1) were generated to match the specifications (of firing rate, population size, and distribution type). For each of the 10 P_0–P_1 pairs, nine additional intermediate morphed patterns were created by morphing through P_0 to P_1. The metrics were computed for all patterns with reference to P_0 and the mean values across the ten sets of patterns were plotted as functions of the morphing parameter β. The metrics used were normalized Euclidean distance (E), Hamming distance (F), cosine similarity (G), and mutual information (H).

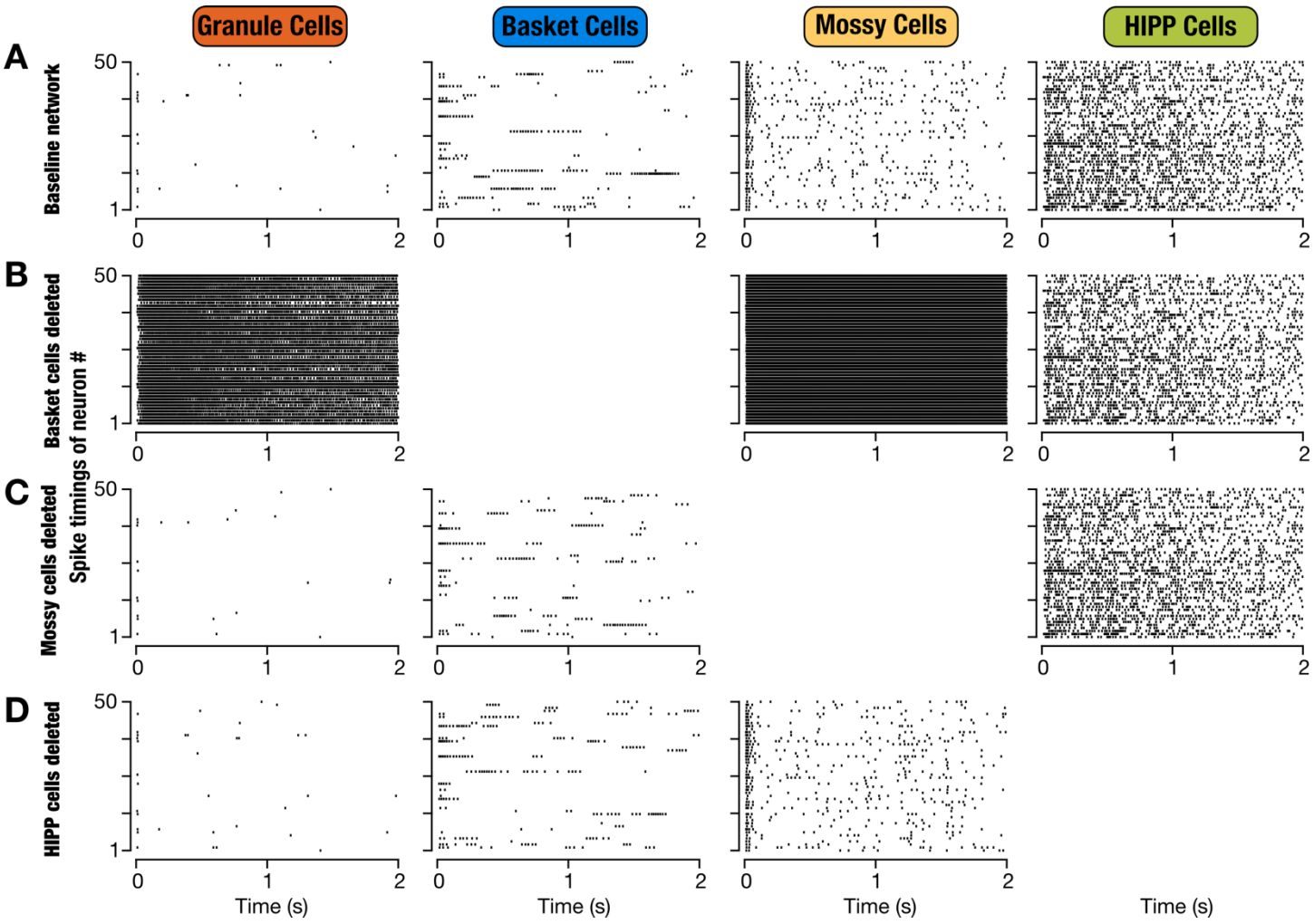

Supplementary Figure S5: Example raster plots from each of the four different cell types in networks where different interneuronal populations were deleted. (A) Raster plots of 50 different granule, basket, mossy, and HIPP cells of the default DG network presented with the P_0 pattern. (B–D) Raster plots of the same cells of the default DG network presented with the P_0 pattern following deletion of basket cells (B), mossy cells (C), or HIPP cells (D).

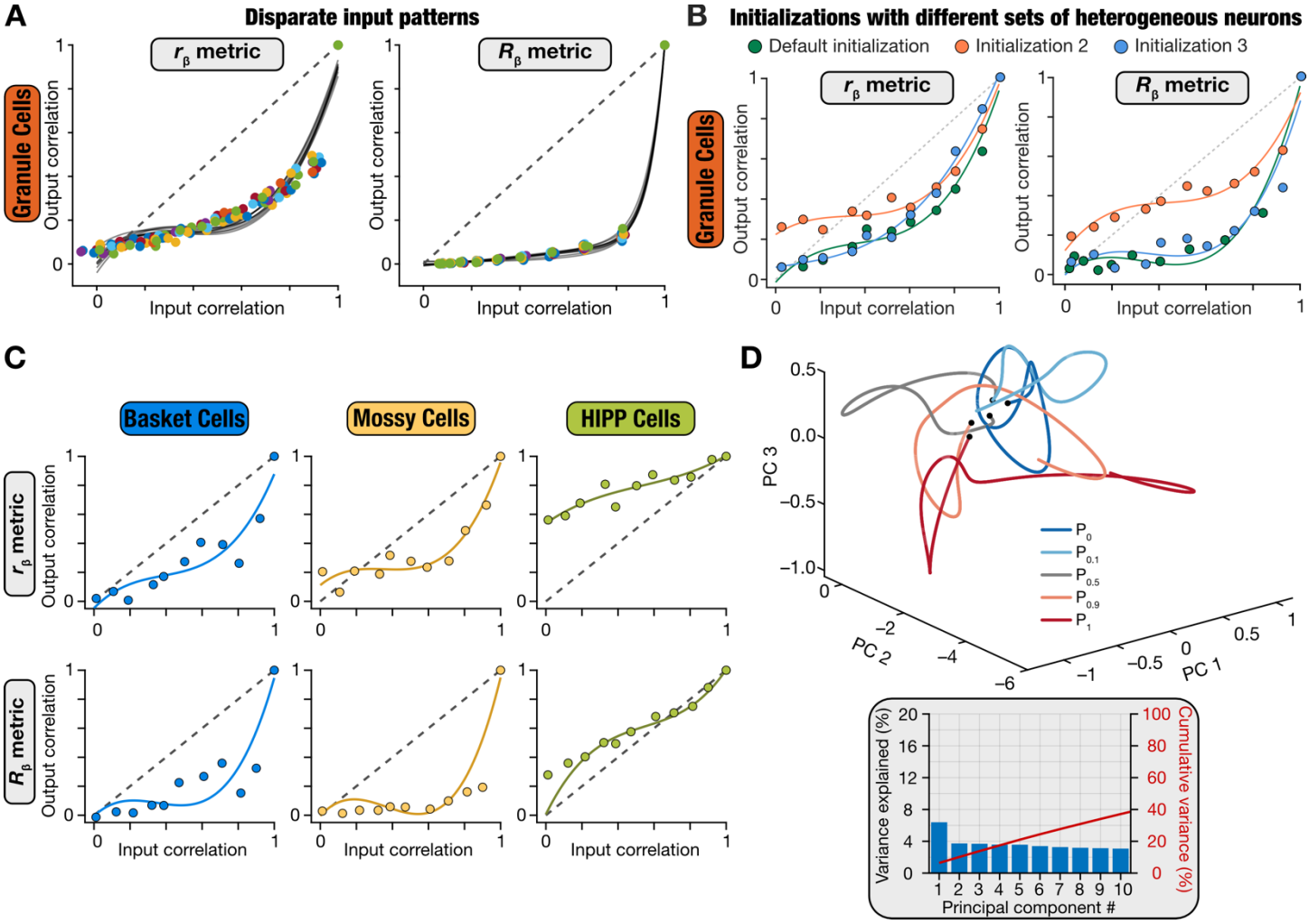

Supplementary Figure S6: Pattern separation performance and dynamics of the default hand-tuned DG network. (A) The hand-tuned DG network was tested with 10 distinct randomly generated input pattern sets. Pattern separation performance was comparable across all patterns, irrespective of whether correlation was computed used quantified using r_β or R_β. These analyses confirmed that the network's pattern separation ability was not restricted to the default input set (shown in Fig. 3). (B) Pattern separation, quantified using the r_β or R_β metrics, for different population initializations of the heterogeneous DG hand-tuned network. In obtaining Initializations 2 and 3, we randomly re-picked heterogeneous neurons from the respective populations, with neuronal choices different from our original default network (Default initialization). We set the synaptic weights to be unchanged across all three networks, the same as our original default network. We presented the 11 morphed patterns to each network, recorded the outputs, computed both r_β and R_β across the input-output patterns of the networks. These results showed that pattern separation was sensitive to the specific initialization of the heterogeneous neuronal population. (C) Pattern decorrelation plots for the basket cell (*left*), mossy cell (*middle*), and HIPP cell (*right*) populations quantified using r_β (*top*) or R_β (*bottom*) metrics for the default input set. (D) The temporal evolution of instantaneous firing rates of the 3600 granule cell population (default network) for 5 different input patterns plotted in a lower-dimensional space using PCA. The black dot marks the start of the trajectory for each case. *Inset*, The variance explained by the first 10 principal components plotted individually and as a cumulative sum. Note the low variance explained by the first 10 dimensions for the sparse and decorrelating DG network.

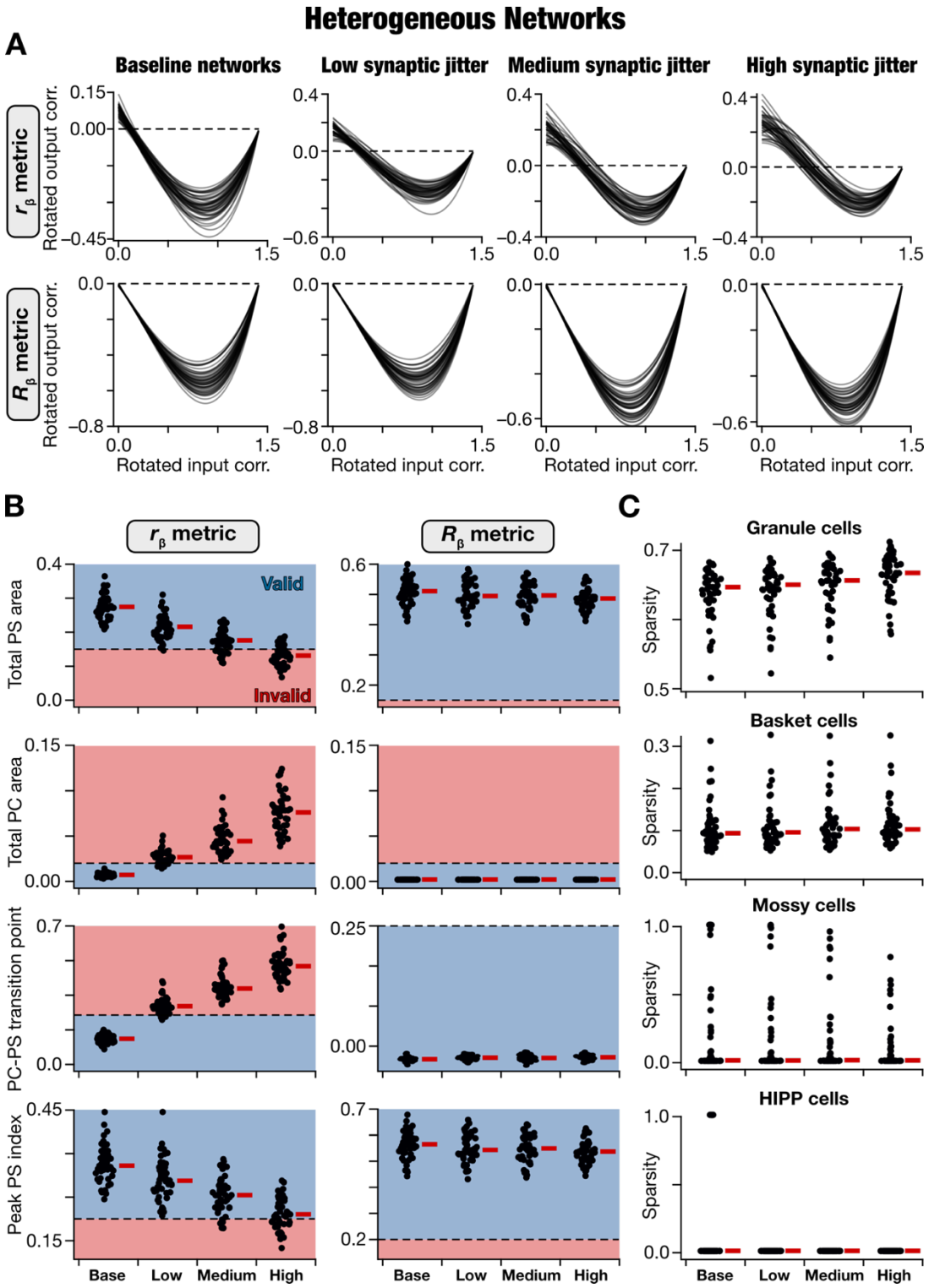

Supplementary Figure S7: Network-to-network variability in the impact of introducing synaptic jitter on pattern separation performance of the 47 valid heterogeneous DG networks. (A) Visualization of pattern separation performance in all 47 valid baseline heterogeneous networks, and in each of the 47 networks with low, medium, and high levels of synaptic jitter. Shown are fitted cubic polynomial on the rotated output correlation *vs*. rotated input correlation datapoints for all 11 morphed patterns. Correlation was computed either with the r_β metric (*top*) or the R_β metric (*bottom*). The pronounced variability in the impact of jitter might be observed across networks. (B) All 4 pattern separation measurements in the valid networks and in networks where different levels of synaptic jitter was introduced. These measurements were calculated from the traces shown in panel A for all 47 networks, with correlation computed either with r_β (*left*) and R_β (*right*). (C) Sparsity of all neuronal subtypes in all 47 valid baseline networks and after introduction of synaptic jitter of different levels. In (B–C), red lines indicate the respective median values.

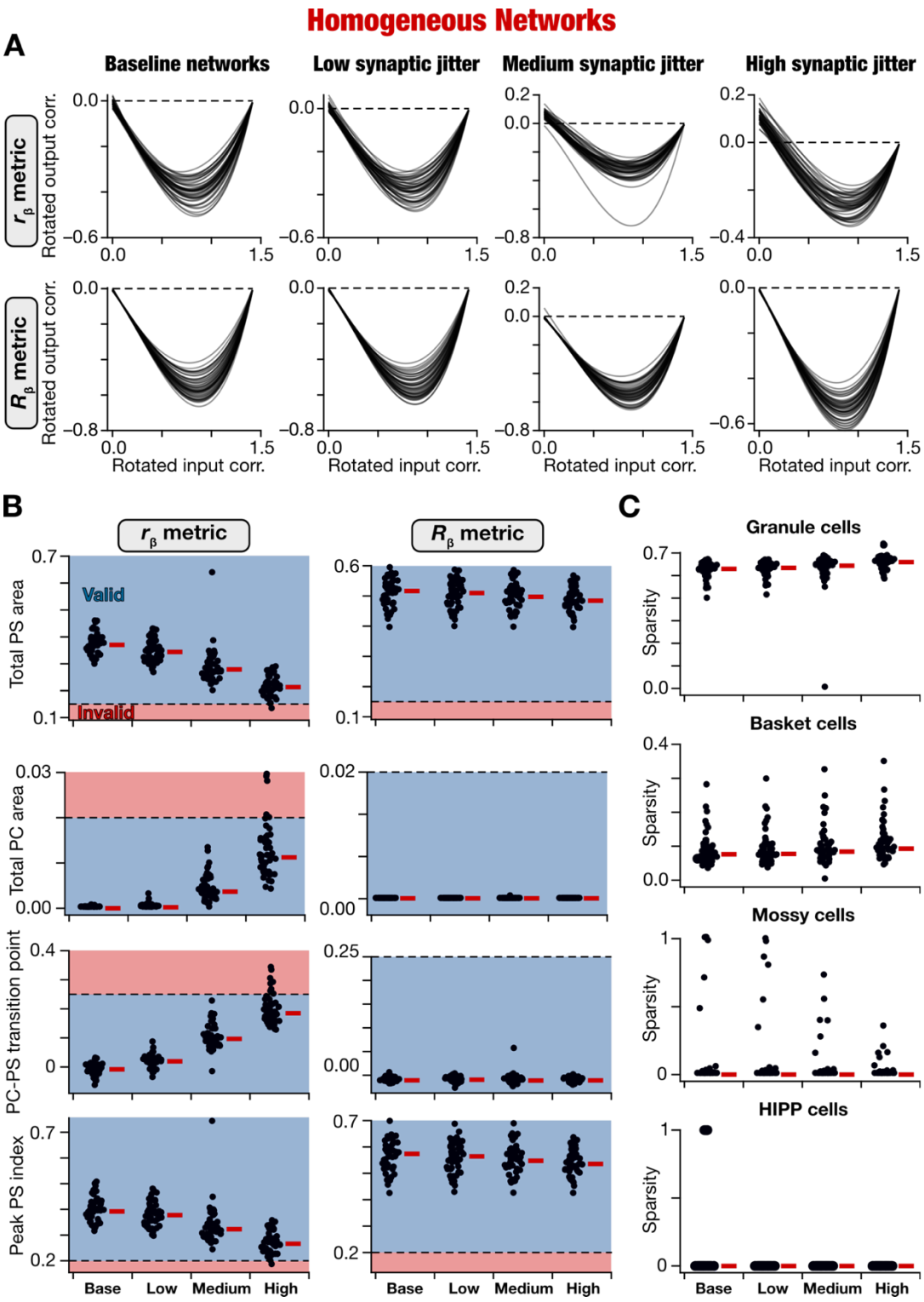

Supplementary Figure S8: Network-to-network variability in the impact of introducing synaptic jitter on pattern separation performance of the 47 valid homogeneous DG networks. (A) Visualization of pattern separation performance in all 47 valid baseline homogeneous networks, and in each of the 47 networks with low, medium, and high levels of synaptic jitter. Shown are fitted cubic polynomial on the rotated output correlation *vs*. rotated input correlation datapoints for all 11 morphed patterns. Correlation was computed either with the r_β metric (*top*) or the R_β metric (*bottom*). The pronounced variability in the impact of jitter might be observed across networks. (B) All 4 pattern separation measurements in the valid networks and in networks where different levels of synaptic jitter was introduced. These measurements were calculated from the traces shown in panel A for all 47 networks, with correlation computed either with r_β (*left*) and R_β (*right*). (C) Sparsity of all neuronal subtypes in all 47 valid baseline networks and after introduction of synaptic jitter of different levels. In (B–C), red lines indicate the respective median values.

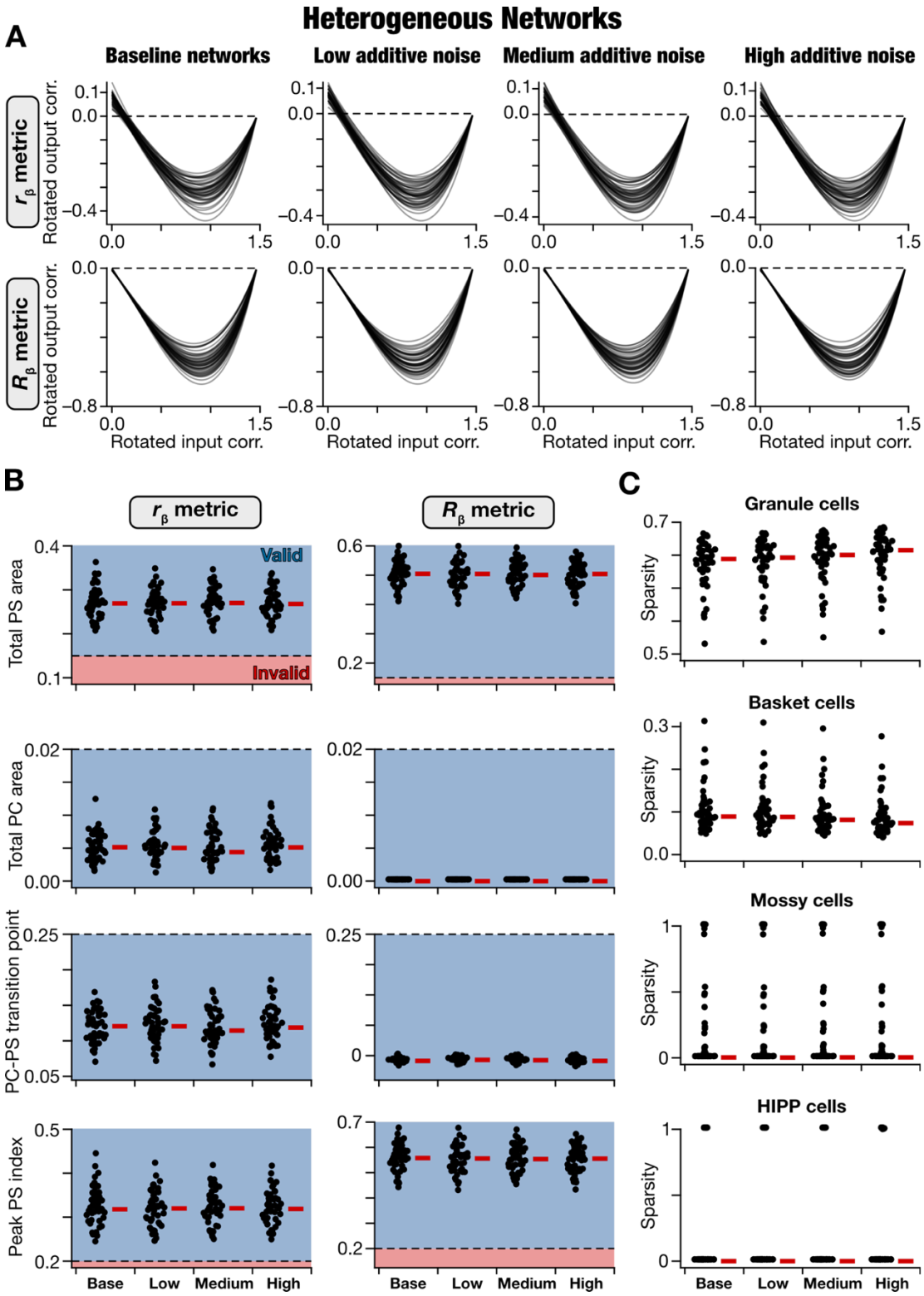

Supplementary Figure S9: Network-to-network variability in the impact of introducing additive noise on pattern separation performance of the 47 valid heterogeneous DG networks. (A) Visualization of pattern separation performance in all 47 valid baseline heterogeneous networks, and in each of the 47 networks with low, medium, and high levels of additive noise. Shown are fitted cubic polynomial on the rotated output correlation *vs*. rotated input correlation datapoints for all 11 morphed patterns. Correlation was computed either with the r_β metric (*top*) or the R_β metric (*bottom*). (B) All 4 pattern separation measurements in the valid networks and in networks where different levels of additive noise was introduced. These measurements were calculated from the traces shown in panel A for all 47 networks, with correlation computed either with r_β (*left*) and R_β (*right*). (C) Sparsity of all neuronal subtypes in all 47 valid baseline networks and after introduction of additive noise of different levels. In (B–C), red lines indicate the respective median values.

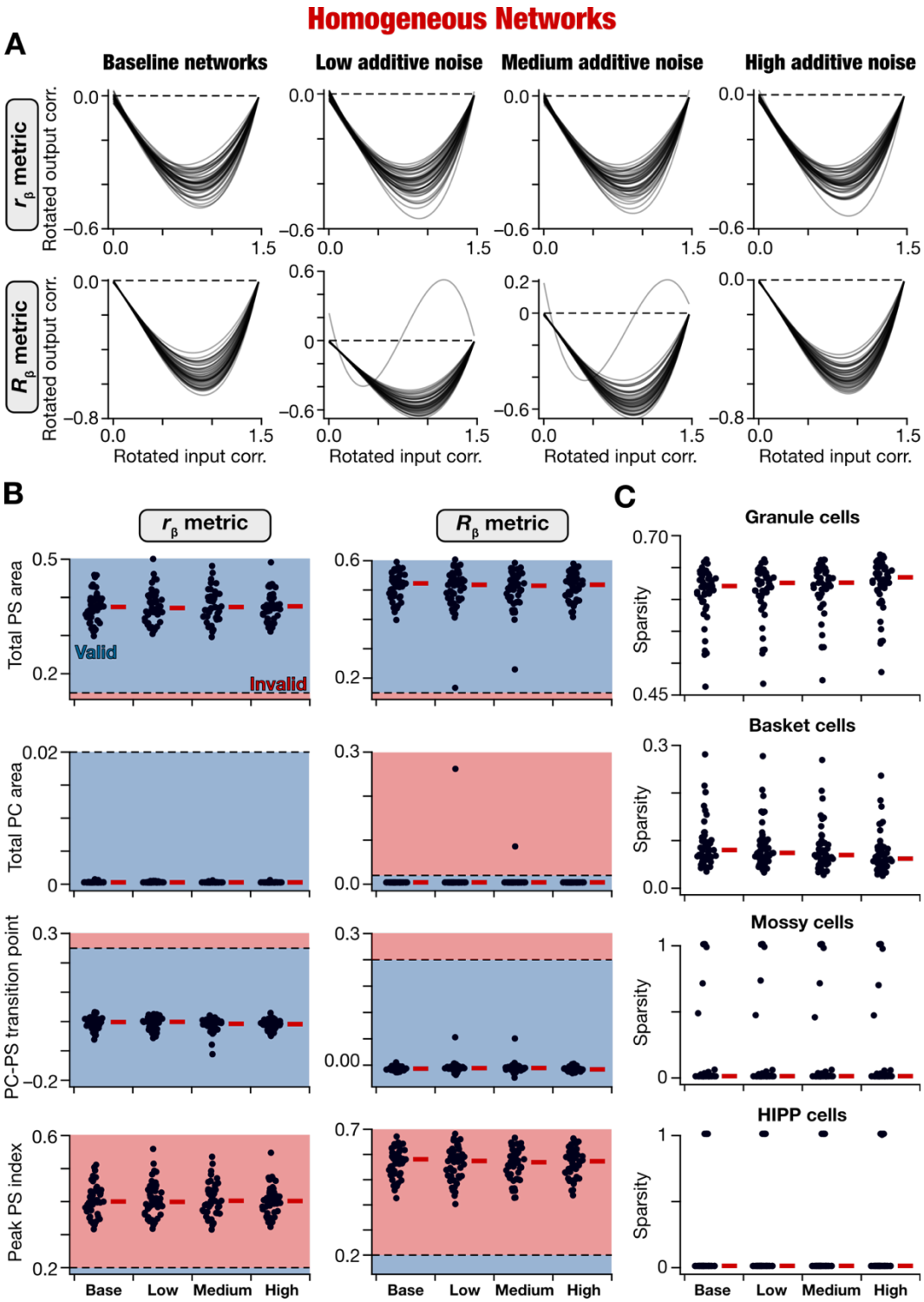

Supplementary Figure S10: Network-to-network variability in the impact of introducing additive noise on pattern separation performance of the 47 valid homogeneous DG networks. (A) Visualization of pattern separation performance in all 47 valid baseline homogeneous networks, and in each of the 47 networks with low, medium, and high levels of additive noise. Shown are fitted cubic polynomial on the rotated output correlation *vs*. rotated input correlation datapoints for all 11 morphed patterns. Correlation was computed either with the r_β metric (*top*) or the R_β metric (*bottom*). The pronounced variability in the impact of noise might be observed across networks. (B) All 4 pattern separation measurements in the valid networks and in networks where different levels of additive noise was introduced. These measurements were calculated from the traces shown in panel A for all 47 networks, with correlation computed either with r_β (*left*) and R_β (*right*). (C) Sparsity of all neuronal subtypes in all 47 valid baseline networks and after introduction of additive noise of different levels. In (B–C), red lines indicate the respective median values.

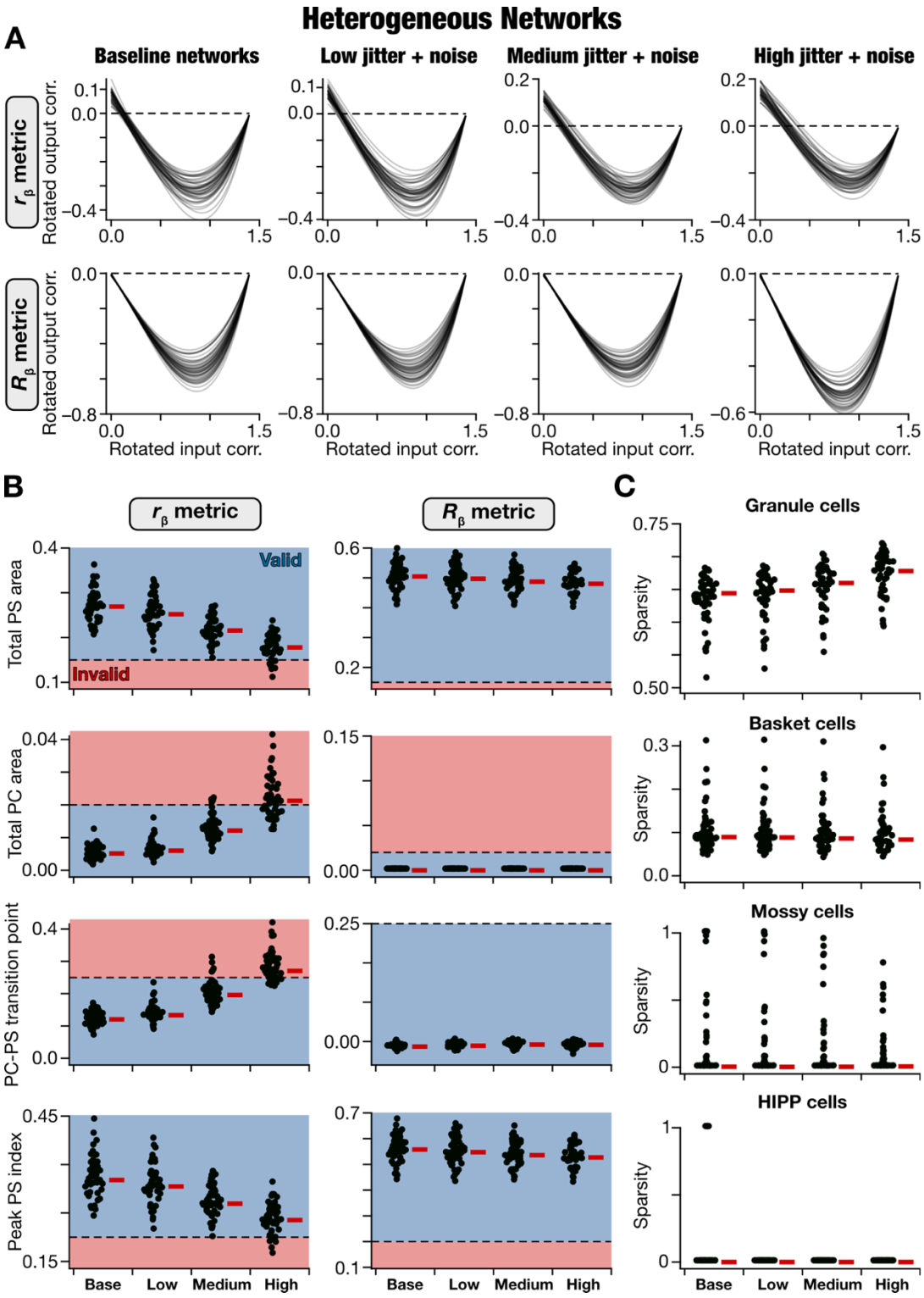

Supplementary Figure S11: Network-to-network variability in the impact of introducing jitter and noise on pattern separation performance of the 47 valid heterogeneous DG networks. (A) Visualization of pattern separation performance in all 47 valid baseline heterogeneous networks, and in each of the 47 networks with low, medium, and high levels of jitter and noise. Shown are fitted cubic polynomial on the rotated output correlation *vs*. rotated input correlation datapoints for all 11 morphed patterns. Correlation was computed either with the r_β metric (*top*) or the R_β metric (*bottom*). The pronounced variability in the impact of jitter and noise might be observed across networks. (B) All 4 pattern separation measurements in the valid networks and in networks where different levels of jitter and noise were introduced. These measurements were calculated from the traces shown in panel A for all 47 networks, with correlation computed either with r_β (*left*) and R_β (*right*). (C) Sparsity of all neuronal subtypes in all 47 valid baseline networks and after introduction of jitter and noise of different levels. In (B–C), red lines indicate the respective median values.

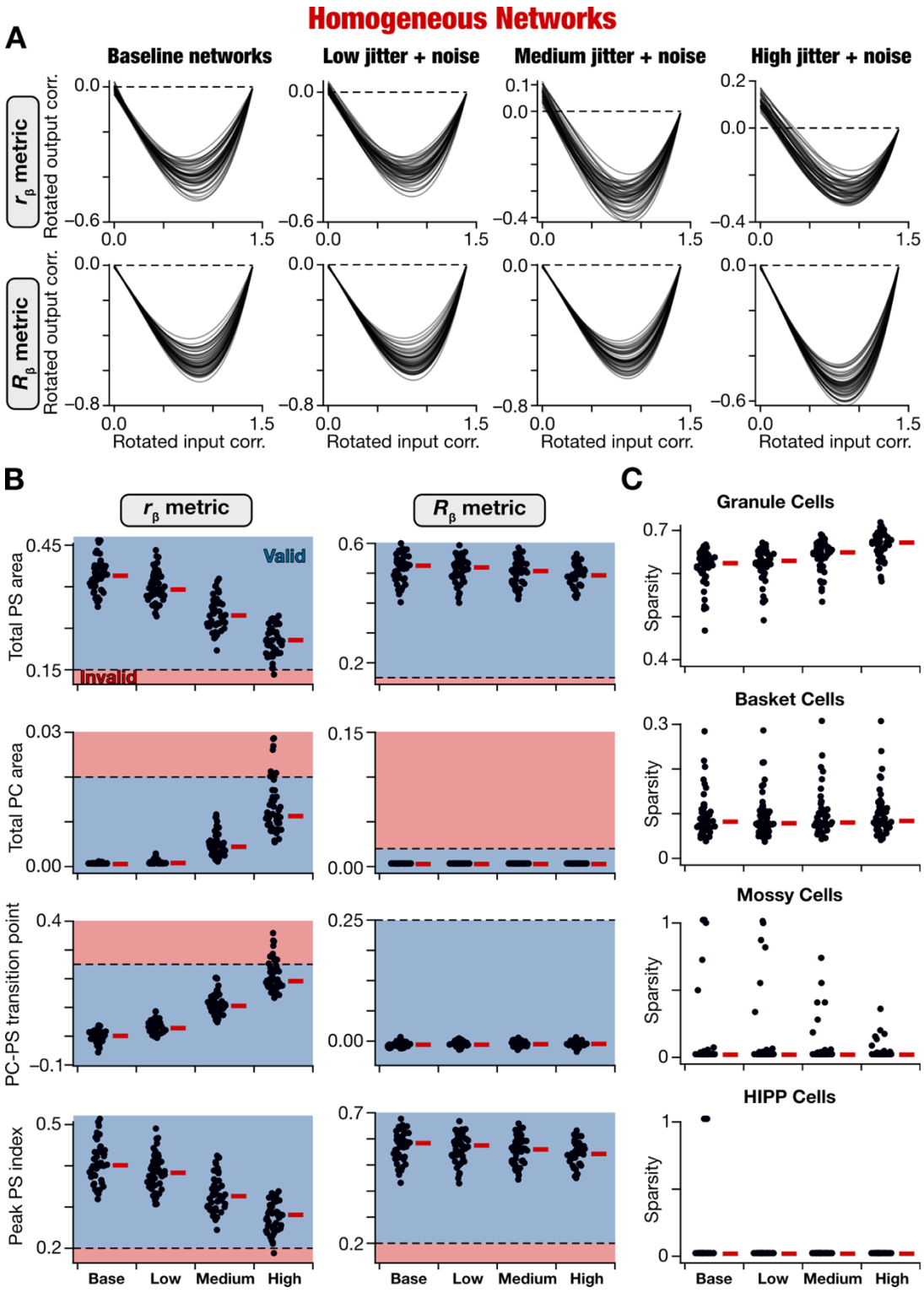

Supplementary Figure S12: Network-to-network variability in the impact of introducing jitter and noise on pattern separation performance of the 47 valid homogeneous DG networks. (A) Visualization of pattern separation performance in all 47 valid baseline homogeneous networks, and in each of the 47 networks with low, medium, and high levels of jitter and noise. Shown are fitted cubic polynomial on the rotated output correlation *vs*. rotated input correlation datapoints for all 11 morphed patterns. Correlation was computed either with the r_β metric (*top*) or the R_β metric (*bottom*). The pronounced variability in the impact of jitter and noise might be observed across networks. (B) All 4 pattern separation measurements in the valid networks and in networks where different levels of jitter and noise were introduced. These measurements were calculated from the traces shown in panel A for all 47 networks, with correlation computed either with r_β (*left*) and R_β (*right*). (C) Sparsity of all neuronal subtypes in all 47 valid baseline networks and after introduction of jitter and noise of different levels. In (B–C), red lines indicate the respective median values.

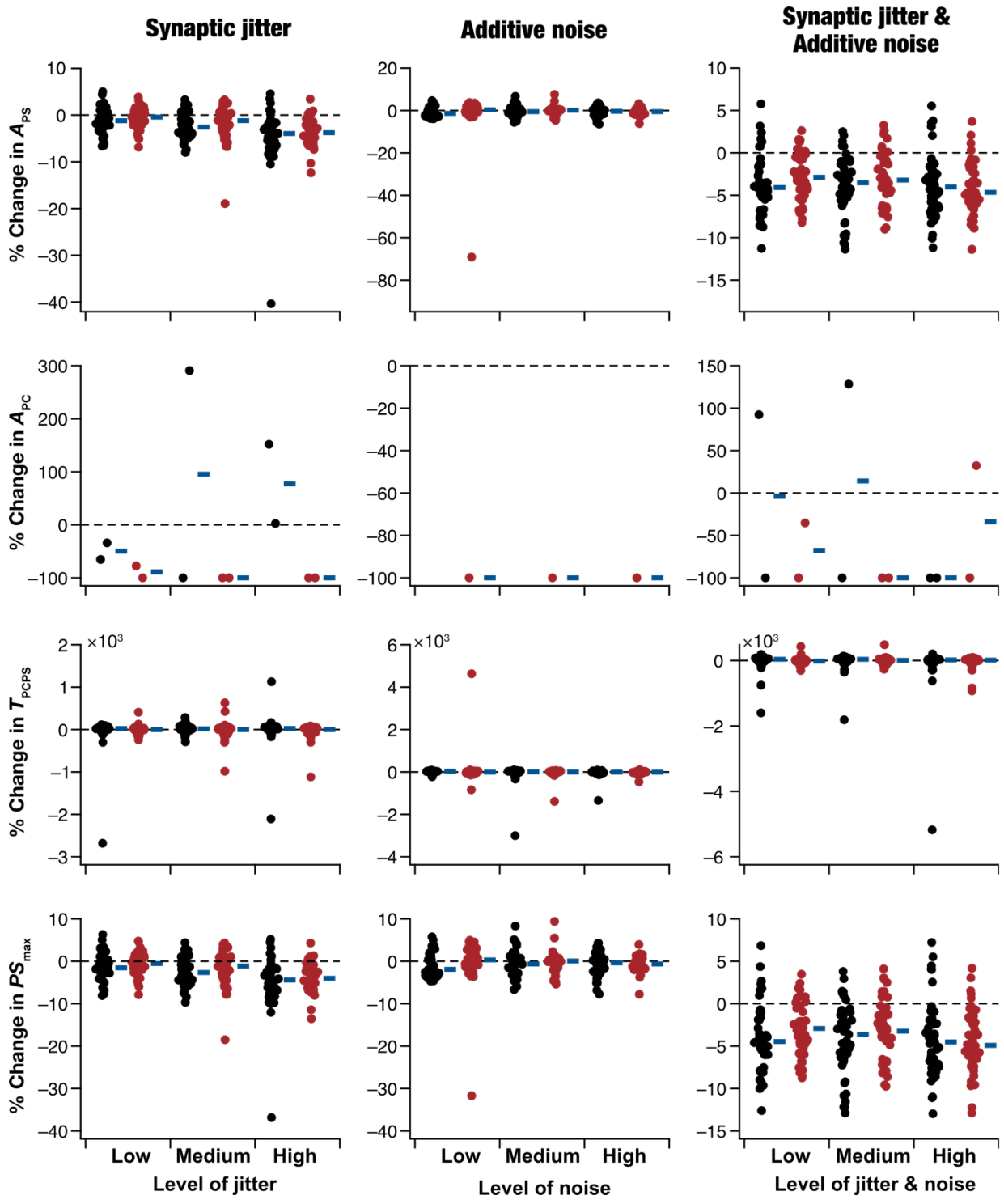

Supplementary Figure S13: Percentage changes in pattern separation measurements computed using R_β in heterogeneous and the homogeneous network challenged with perturbations. Percentage changes in pattern separation measurements (computed using the R_β metric) when perturbations of different levels were introduced. Percentage changes were computed with reference to the base networks where there were no perturbations. Perturbations were introduced in three distinct levels (low, medium, and high) as synaptic jitter (*left column*), or as additive noise to synaptic currents (*middle column*) or a combination of both jitter and noise (*right column*). The pronounced network-to-network variability, in both homogeneous and heterogeneous networks, in percentage changes of pattern separation measurements for the same levels of jitter and/or noise may be noted. In all plots, blue lines indicate the respective median values. The changes in the different measurements for the heterogeneous *vs*. homogeneous networks were not significantly different (Wilcox rank sum test).

Supplementary Table S1. Base values and ranges for all the parameters used for generating a heterogeneous population for granule cells.

Granule cells				
Symbol	**Parameter**	**Base Model**	**Lower Bound**	**Upper Bound**
$E_l\ (mV)$	Resting Potential	–75	–77	–73
$R_m\ (k\Omega\ cm^2)$	Specific membrane resistance	38	30	42
$C_m\ (\mu F/cm^2\ )$	Specific membrane capacitance	1	1	1
$\tau_w\ (ms)$	Adaptation time constant	300	200	500
$\alpha\ (nS)$	Adaptation coupling parameter	0.40	0	3
$b\ (pA)$	Spike trigger parameter	15	5	25
$\Delta_T\ (mV)$	Slope Factor	5	0	10
$V_{Reset}\ (mV)$	Reset Voltage	–77	–80	–75
$V_{th}\ (mV)$	Threshold voltage	–60	–65	–57
$A\ (\mu m^2)$	Area	30	20	40

Supplementary Table S2. Base values and ranges for all the parameters used for generating a heterogeneous population for basket cells.

Basket cells				
Symbol	**Parameter**	**Base Model**	**Lower Bound**	**Upper Bound**
$E_l\ (mV)$	Resting Potential	–65	–67	–63
$R_m\ (k\Omega\ cm^2)$	Specific membrane resistance	8	5	10
$C_m\ (\mu F/cm^2\ )$	Specific membrane capacitance	1	1	1
$\tau_w\ (ms)$	Adaptation time constant	80	20	100
$\alpha\ (nS)$	Adaptation coupling parameter	1.5	0	3
$b\ (pA)$	Spike trigger parameter	2	0	8
$\Delta_T\ (mV)$	Slope Factor	2	0	4
$V_{Reset}\ (mV)$	Reset Voltage	–70	–73	–65
$V_{th}\ (mV)$	Threshold voltage	–57	–63	–57
$A\ (\mu m^2)$	Area	13	10	14

Supplementary Table S3. Base values and ranges for all the parameters used for generating a heterogeneous population for mossy cells.

Mossy cells				
Symbol	**Parameter**	**Base Model**	**Lower Bound**	**Upper Bound**
$E_l\ (mV)$	Resting Potential	–61	–63	–58
$R_m\ (k\Omega\ cm^2)$	Specific membrane resistance	43	41	48
$C_m\ (\mu F/cm^2\ )$	Specific membrane capacitance	1	1	1
$\tau_w\ (ms)$	Adaptation time constant	400	100	500
$\alpha\ (nS)$	Adaptation coupling parameter	0.8	0	3
$b\ (pA)$	Spike trigger parameter	50	10	70
$\Delta_T\ (mV)$	Slope Factor	1	0	10
$V_{Reset}\ (mV)$	Reset Voltage	–65	–67	–63
$V_{th}\ (mV)$	Threshold voltage	–47	–40	–32
$A\ (\mu m^2)$	Area	17	10	18

Supplementary Table S4. Base values and ranges for all the parameters used for generating a heterogeneous population for HIPP cells.

HIPP Cells				
Symbol	**Parameter**	**Base Model**	**Lower Bound**	**Upper Bound**
$E_l\ (mV)$	Resting Potential	–60	–63	–58
$R_m\ (k\Omega\ cm^2)$	Specific membrane resistance	24	22	26
$C_m\ (\mu F/cm^2\ )$	Specific membrane capacitance	1	1	1
$\tau_w\ (ms)$	Adaptation time constant	115	50	300
$\alpha\ (nS)$	Adaptation coupling parameter	0.6	0	3
$b\ (pA)$	Spike trigger parameter	40	10	70
$\Delta_T\ (mV)$	Slope Factor	2	0	10
$V_{Reset}\ (mV)$	Reset Voltage	–55	–58	–53
$V_{th}\ (mV)$	Threshold voltage	–42	–45	–39
$A\ (\mu m^2)$	Area	4	3	10

Supplementary Table S5. Bounds for the physiologically relevant measurements for all four neuronal subtypes.

Symbol	Measurement	Lower Bound	Upper Bound
Granule Cells			
$\tau_m\ (ms)$	Membrane time constant	26	35
Sag	Sag ratio	0.9	1
$R_{in}\ (M\Omega)$	Input resistance	107	228
$f_{50}\ (Hz)$	Firing frequency when 50 pA current is injected	0	0
$f_{150}\ (Hz)$	Firing frequency when 150 pA current is injected	10	15
SFA	Spike frequency adaptation	0.1	0.8
Basket Cells			
$\tau_m\ (ms)$	Membrane time constant	6	10
Sag	Sag ratio	0.9	1
$R_{in}\ (M\Omega)$	Input resistance	45	65
$f_{50}\ (Hz)$	Firing frequency when 50 pA current is injected	0	0
$f_{150}\ (Hz)$	Firing frequency when 150 pA current is injected	30	50
SFA	Spike frequency adaptation	0.85	1
Mossy Cells			
$\tau_m\ (ms)$	Membrane time constant	26	**32**
Sag	Sag ratio	0.6	0.91
$R_{in}\ (M\Omega)$	Input resistance	180	250
$f_{50}\ (Hz)$	Firing frequency when 50 pA current is injected	0	0
$f_{150}\ (Hz)$	Firing frequency when 150 pA current is injected	5	10
SFA	Spike frequency adaptation	0.2	0.8
HIPP Cells			
$\tau_m\ (ms)$	Membrane time constant	14	20
Sag	Sag ratio	0.5	0.95
$R_{in}\ (M\Omega)$	Input resistance	320	420
$f_{50}\ (Hz)$	Firing frequency when 50 pA current is injected	0	5
$f_{150}\ (Hz)$	Firing frequency when 150 pA current is injected	20	30
SFA	Spike frequency adaptation	0.05	0.8

Supplementary Table S6: Connection probability of different synaptic connections in the network. Rows represent presynaptic and columns represent postsynaptic cell [1].

		Postsynaptic cells				
		PP	**Granule**	**HIPP**	**Mossy**	**Basket**
Presynaptic cells	**PP**	–	0.015	0.035	–	–
	Granule	–	–	–	0.02	0.018
	HIPP	–	0.12	–	–	–
	Mossy	–	0.05	–	–	0.05
	Basket	–	0.16	–	–	–

Supplementary Table S7: Rise and decay time constant along with synaptic reversal potential for all the synapses in the network, synaptic weights and axon delays [1-5].

Synapse (Pre → Post)	τ_{rise} (ms)	τ_{decay} (ms)	E_{syn} (mV)	$\bar{g}_{syn}$ (nS)	**Axon delay (ms)**
AMPA					
PP → GC	0.1	2.5	0	6.43	3.0
GC → MC	0.5	6.5	0	2.85	1.5
GC → BC	2.5	3.5	0	5.47	0.8
PP → HIPP	2.0	11.0	0	1.98	3.0
MC → GC	0.1	2.5	0	4.35	3.0
MC → BC	2.5	3.5	0	2.13	3.0
NMDA					
PP → GC	0.33	50.0	0	6.944	3.0
PP → HIPP	4.8	110.0	0	2.138	3.0
GC → MC	4.0	100.0	0	3.078	1.5
MC → GC	0.33	55.0	0	4.698	3.0
MC → BC	10.0	130.0	0	2.300	3.0
GC → BC	10.0	130.0	0	5.852	0.8
GABA					
BC → GC	0.9	6.8	–90	4.29	0.85
HIPP → GC	0.9	6.8	–90	2.65	1.6

Supplementary Table S8: Parametric bounds for the 8 synaptic weights for running MPMOSS to obtain valid DG networks.

Pre → Post	Symbol	Lower Bound (nS)	Upper Bound (nS)
PP → Granule	W_{GP}	0	20
PP → HIPP	W_{HP}	0	10
HIPP → Granule	W_{GH}	0	10
Granule → Mossy	W_{MG}	0	10
Granule → Basket	W_{BG}	0	10
Mossy → Granule	W_{GM}	0	10
Mossy → Basket	W_{BM}	0	10
Basket → Granule	W_{GB}	0	10

Supplementary Table S9: Measurements bounds used for the validation of networks that were effective in performing pattern separation.

Measurement	Description	Range
$\boldsymbol{A_{\mathrm{PS}}}$	Total pattern separation area	> 0.15
$\boldsymbol{A_{\mathrm{PC}}}$	Total pattern completion area	< 0.02
$\boldsymbol{T_{\mathrm{PCPS}}}$	Pattern completion to pattern separation transition point	< 0.25
$\boldsymbol{PS_{\max}}$	Peak pattern separation index	> 0.2

Supplementary Table S10: Outcomes of statistical tests for data in Figure 6.

Panel	Measurement	Groups	Test used	p value
Figure 6B	$A_{PS}\ (r_\beta)$	Base, BC⁻, MC⁻, HC⁻	Kruskal Wallis	$< 2.2 \times 10^{-16}$
Figure 6B	$A_{PS}\ (r_\beta)$	Base *vs.* BC⁻ Base *vs.* MC⁻ Base *vs.* HC⁻	Wilcox signed rank	1.4×10^{-14} 0.20 0.02
Figure 6B	$A_{PC}\ (r_\beta)$	Base, BC⁻, MC⁻, HC⁻	Kruskal Wallis	1.6×10^{-13}
Figure 6B	$A_{PC}\ (r_\beta)$	Base *vs.* BC⁻ Base *vs.* MC⁻ Base *vs.* HC⁻	Wilcox signed rank	1.4×10^{-14} 0.16 8.2×10^{-3}
Figure 6B	$T_{PCPS}\ (r_\beta)$	Base, BC⁻, MC⁻, HC⁻	Kruskal Wallis	3.4×10^{-8}
Figure 6B	$T_{PCPS}\ (r_\beta)$	Base *vs.* BC⁻ Base *vs.* MC⁻ Base *vs.* HC⁻	Wilcox signed rank	1.5×10^{-5} 5.3×10^{-4} 1.8×10^{-4}
Figure 6B	$PS_{\max}\ (r_\beta)$	Base, BC⁻, MC⁻, HC⁻	Kruskal Wallis	$< 2.2 \times 10^{-16}$
Figure 6B	$PS_{\max}\ (r_\beta)$	Base *vs.* BC⁻ Base *vs.* MC⁻ Base *vs.* HC⁻	Wilcox signed rank	1.4×10^{-14} 0.08 6.7×10^{-3}
Figure 6B	$A_{PS}\ (R_\beta)$	Base, BC⁻, MC⁻, HC⁻	Kruskal Wallis	$< 2.2 \times 10^{-16}$
Figure 6B	$A_{PS}\ (R_\beta)$	Base *vs.* BC⁻ Base *vs.* MC⁻ Base *vs.* HC⁻	Wilcox signed rank	2.8×10^{-14} 6.2×10^{-10} 3.0×10^{-11}
Figure 6B	$A_{PC}\ (R_\beta)$	Base, BC⁻, MC⁻, HC⁻	Kruskal Wallis	$< 2.2 \times 10^{-16}$
Figure 6B	$A_{PC}\ (R_\beta)$	Base *vs.* BC⁻ Base *vs.* MC⁻ Base *vs.* HC⁻	Wilcox signed rank	5.7×10^{-14} 6.5×10^{-5} 4.5×10^{-6}
Figure 6B	$T_{PCPS}\ (R_\beta)$	Base, BC⁻, MC⁻, HC⁻	Kruskal Wallis	$< 2.2 \times 10^{-16}$
Figure 6B	$T_{PCPS}\ (R_\beta)$	Base *vs.* BC⁻ Base *vs.* MC⁻ Base *vs.* HC⁻	Wilcox signed rank	5.8×10^{-11} 0.07 5.4×10^{-3}
Figure 6B	$PS_{\max}\ (R_\beta)$	Base, BC⁻, MC⁻, HC⁻	Kruskal Wallis	$< 2.2 \times 10^{-16}$
Figure 6B	$PS_{\max}\ (R_\beta)$	Base *vs.* BC⁻ Base *vs.* MC⁻ Base *vs.* HC⁻	Wilcox signed rank	5.4×10^{-10} 1.8×10^{-7} 2.9×10^{-9}
Figure 6C	$Sparsity$ (GCs)	Base, BC⁻, MC⁻, HC⁻	Kruskal Wallis	$< 2.2 \times 10^{-16}$
Figure 6C	$Sparsity$ (GCs)	Base *vs.* BC⁻ Base *vs.* MC⁻ Base *vs.* HC⁻	Wilcox signed rank	2.5×10^{-9} 7.1×10^{-14} 7.1×10^{-14}
Figure 6C	$Sparsity$ (BCs)	Base, MC⁻, HC⁻	Kruskal Wallis	$< 2.2 \times 10^{-16}$
Figure 6C	$Sparsity$ (BCs)	Base *vs.* MC⁻ Base *vs.* HC⁻	Wilcox signed rank	2.5×10^{-9} 2.5×10^{-9}
Figure 6C	$Sparsity$ (MCs)	Base, BC⁻, HC⁻	Kruskal Wallis	$< 2.2 \times 10^{-16}$
Figure 6C	$Sparsity$ (MCs)	Base *vs.* BC⁻ Base *vs.* HC⁻	Wilcox signed rank	1.2×10^{-6} 1.2×10^{-6}
Figure 6C	$Sparsity$ (HIPP)	Base, BC⁻, MC⁻	Kruskal Wallis	0.65
Figure 6C	$Sparsity$ (HIPP)	Base *vs.* BC⁻ Base *vs.* MC⁻	Wilcox signed rank	0.18 0.18

Supplementary Table S11: Outcomes of statistical tests for data in Figure 7.

Measurement	Groups	Test used	p value
Synaptic jitter			
Change in A_{PS}	Low jitter Homogeneous *vs.* Heterogeneous	Wilcox rank sum	1.0×10^{-13}
Change in A_{PS}	Medium jitter Homogeneous *vs.* Heterogeneous	Wilcox rank sum	1.7×10^{-16}
Change in A_{PS}	High jitter Homogeneous *vs.* Heterogeneous	Wilcox rank sum	7.3×10^{-19}
Change in A_{PC}	Low jitter Homogeneous *vs.* Heterogeneous	Wilcox rank sum	3.3×10^{-3}
Change in A_{PC}	Medium jitter Homogeneous *vs.* Heterogeneous	Wilcox rank sum	4.0×10^{-16}
Change in A_{PC}	High jitter Homogeneous *vs.* Heterogeneous	Wilcox rank sum	4.0×10^{-16}
Change in T_{PCPS}	Low jitter Homogeneous *vs.* Heterogeneous	Wilcox rank sum	7.0×10^{-10}
Change in T_{PCPS}	Medium jitter Homogeneous *vs.* Heterogeneous	Wilcox rank sum	1.2×10^{-27}
Change in T_{PCPS}	High jitter Homogeneous *vs.* Heterogeneous	Wilcox rank sum	1.2×10^{-27}
Change in $PS_{\max}$	Low jitter Homogeneous *vs.* Heterogeneous	Wilcox rank sum	1.0×10^{-6}
Change in $PS_{\max}$	Medium jitter Homogeneous *vs.* Heterogeneous	Wilcox rank sum	8.4×10^{-10}
Change in $PS_{\max}$	High jitter Homogeneous *vs.* Heterogeneous	Wilcox rank sum	1.8×10^{-12}

Supplementary Table S11: Outcomes of statistical tests for data in Figure 7 (contd).

Measurement	Groups	Test used	p value
Additive noise			
Change in A_{PS}	Low noise Homogeneous *vs.* Heterogeneous	Wilcox rank sum	0.28
Change in A_{PS}	Medium noise Homogeneous *vs.* Heterogeneous	Wilcox rank sum	0.96
Change in A_{PS}	High noise Homogeneous *vs.* Heterogeneous	Wilcox rank sum	0.94
Change in A_{PC}	Low noise Homogeneous *vs.* Heterogeneous	Wilcox rank sum	2.9×10^{-3}
Change in A_{PC}	Medium noise Homogeneous *vs.* Heterogeneous	Wilcox rank sum	$< 2.2 \times 10^{-5}$
Change in A_{PC}	High noise Homogeneous *vs.* Heterogeneous	Wilcox rank sum	1.2×10^{-6}
Change in T_{PCPS}	Low noise Homogeneous *vs.* Heterogeneous	Wilcox rank sum	0.76
Change in T_{PCPS}	Medium noise Homogeneous *vs.* Heterogeneous	Wilcox rank sum	0.43
Change in T_{PCPS}	High noise Homogeneous *vs.* Heterogeneous	Wilcox rank sum	0.91
Change in $PS_{\max}$	Low noise Homogeneous *vs.* Heterogeneous	Wilcox rank sum	0.20
Change in $PS_{\max}$	Medium noise Homogeneous *vs.* Heterogeneous	Wilcox rank sum	0.98
Change in $PS_{\max}$	High noise Homogeneous *vs.* Heterogeneous	Wilcox rank sum	0.43

Supplementary Table S11: Outcomes of statistical tests for data in Figure 7 (contd).

Measurement	Groups	Test used	p value
Synaptic jitter & Additive noise			
Change in A_{PS}	Low jitter & noise Homogeneous *vs.* Heterogeneous	Wilcox rank sum	0.03
Change in A_{PS}	Medium jitter & noise Homogeneous *vs.* Heterogeneous	Wilcox rank sum	4.1×10^{-5}
Change in A_{PS}	High jitter & noise Homogeneous *vs.* Heterogeneous	Wilcox rank sum	1.6×10^{-5}
Change in A_{PC}	Low jitter & noise Homogeneous *vs.* Heterogeneous	Wilcox rank sum	0.04
Change in A_{PC}	Medium jitter & noise Homogeneous *vs.* Heterogeneous	Wilcox rank sum	8.4×10^{-13}
Change in A_{PC}	High jitter & noise Homogeneous *vs.* Heterogeneous	Wilcox rank sum	4.0×10^{-16}
Change in T_{PCPS}	Low jitter & noise Homogeneous *vs.* Heterogeneous	Wilcox rank sum	0.04
Change in T_{PCPS}	Medium jitter & noise Homogeneous *vs.* Heterogeneous	Wilcox rank sum	7.1×10^{-16}
Change in T_{PCPS}	High jitter & noise Homogeneous *vs.* Heterogeneous	Wilcox rank sum	9.0×10^{-24}
Change in $PS_{\max}$	Low jitter & noise Homogeneous *vs.* Heterogeneous	Wilcox rank sum	0.09
Change in $PS_{\max}$	Medium jitter & noise Homogeneous *vs.* Heterogeneous	Wilcox rank sum	2.9×10^{-4}
Change in $PS_{\max}$	High jitter & noise Homogeneous *vs.* Heterogeneous	Wilcox rank sum	7.7×10^{-5}

Supplementary References

1. Chavlis S, Petrantonakis PC, Poirazi P. Dendrites of dentate gyrus granule cells contribute to pattern separation by controlling sparsity. *Hippocampus.* 2017;27 (1):89-110. doi: 10.1002/hipo.22675.
2. Geiger JR, Lübke J, Roth A, Frotscher M, Jonas P. Submillisecond AMPA receptor-mediated signaling at a principal neuron–interneuron synapse. *Neuron.* 1997;18 (6):1009-1023. https://www.sciencedirect.com/science/article/pii/S0896627300803396.
3. Bartos M, Vida I, Frotscher M, Geiger JR, Jonas P. Rapid signaling at inhibitory synapses in a dentate gyrus interneuron network. *J Neurosci.* 2001;21 (8):2687-2698. http://www.ncbi.nlm.nih.gov/pubmed/11306622.
4. Larimer P, Strowbridge BW. Nonrandom local circuits in the dentate gyrus. *Journal of Neuroscience.* 2008;28 (47):12212-12223. doi: 10.1523/JNEUROSCI.3612-08.2008.
5. Myers CE, Scharfman HE. A role for hilar cells in pattern separation in the dentate gyrus: a computational approach. *Hippocampus.* 2009;19 (4):321-337. doi: 10.1002/hipo.20516.